01 E 02 DEZEMBRO
POSMEC 1986–2016

POSMEC 2016 – Postgraduate Symposium in Mechanical Engineering
Department of Mechanical Engineering – Federal University of Uberlandia
December, 1st to 2nd, Uberlandia, Minas Gerais, Brazil

FEM DYNAMIC ANALYSIS OF AN ONBOARD ROTOR

Marcelo Samora Sousa Jr, Federal University of Uberlândia, marcelosamora@ufu.br
Vergílio T. S. Del Claro, Federal University of Uberlândia, vergiliotorezan@gmail.com
Aldemir Aparecido Cavalini Jr, Federal University of Uberlândia, aacjunior@ufu.br
Valder Steffen, Federal University of Uberlândia, vsteffen@ufu.br

Abstract: *A FEM study regarding the dynamic behavior of rotating machines subject to base excitation and unbalance forces is hereby presented. The mathematical model of the rotor is based on the Timoshenko beam theory, which is obtained by considering the strain and kinetic energies of the shaft, discs, and mass unbalance. The resulting equations are used to provide information about the vibration responses of the rotor under base and unbalance excitations simultaneously. Some simplifications are adopted in order to obtain the responses of the considered rotor system, which is composed by a horizontal flexible shaft, two rigid discs, and two self-alignment ball bearings. Therefore, the proposed analysis is performed both in time and frequency domains, as illustrated by the orbits, unbalance response, and the Campbell diagram of the rotating machine. Finally, this study illustrates the main dynamic phenomena associated with onboard rotor systems.*

Keywords*: onboard rotors, FEM model, vibration responses.*

1. INTRODUCTION

Due to the rotating characteristic of shafts and rotating machines, these occasionally introduce mechanical energy, originated from unbalances, to a given system. These may be fixed or onboard rotors, as hydroelectric turbines, turbofan turbines, compressors, etc.. These rotating machines tend to operate at a very high speed, making the comprehension of the dynamic behavior and influential parameters an essential step to the improvement of their performance and functionalities. In this sense, the study of rotating machines enables a better control and increased performances, ranges of operation and definition of better operating regimes for these mechanisms.

Contrary to what has been initially concluded by Rankine (1896), a rotating machine may operate at a speed superior to its critical speed (Dunkerley, 1984). As the studies on the theme evolved, the critical speed became a crucial parameter for projects and parametrizations. Machines that operate beyond the critical speed need to first get past it to reach the ideal operating speed, which demands additional energy and control systems to resist possible resonance effects. This becomes a project consideration, influencing strongly on structural dimensioning and also in the machines performance. Another condition that allows for a better understanding of rotors in the variation on the vibration amplitude on the critical speed. The Campbell Diagram, developed by Wilfred Campbell, is a great auxiliary tool for the comprehension of rotors theory and represents the rotors natural frequencies considering the influence of the rotating speed.

Even before the widespread use of the Finite Elements Method (FEM) in rotating machines, the Transference Matrix logic that considered a continuous system, developed by Lallement, Lecoanet and Steffen Jr. (1982), brought concepts that evolved with the FEM. The greater computational capacity and data processing capability made possible the implementation of a greater number of variables in the mechanical models, bringing the approximations to a minimum and increasing the realism and precision of the simulations of case studies. Thus, effects like rotating inertia, axial forces and gyroscopic moments were introduced to the FEM models by Nelson and MacVaugh (1976), accordingly to Ishida and Yamamoto (2012).

In this context, the present study aims to better understand the influence of a range of new parameters and study the dynamic behavior of rotors. The study is based on a horizontal test rig, composed by a flexible shaft and two rigid discs, mounted on two ball bearings, which are the reference parameters used for the FEM model. The methodology used is the consideration of flexibility in the Lagrange equations, used simultaneously with a FEM model. This model is satisfactorily similar to the real system, accordingly to Lalanne and Ferraris (1998), as the rotating machines dynamic behavior is described in a pertinent sense. The kinetic energy of the discs, the unbalanced mass and the shaft are considered in their modelling. For the shaft, the strain energy is also considered, which introduces its characteristic flexibility in the model. As for the mechanical seals that introduce a local stiffness, it is used a virtual work equation. During the evaluation of the numerical model its results were compared to experimental results, obtained through the test rig, which allowed a better understanding of the systems dynamic behavior.

2. ROTOR MODELING

Figure (1) shows the schematic representation of the onboard rotor in which three reference frames are used (Duchemin, Berlioz, Ferraris, 2006). $R_0(x_0, y_0, z_0)$ is the inertial frame, $R_s(x_s, y_s, z_s)$ is the frame fixed to the rotor base, and $R(x, y, z)$ is the frame fixed to the disc.

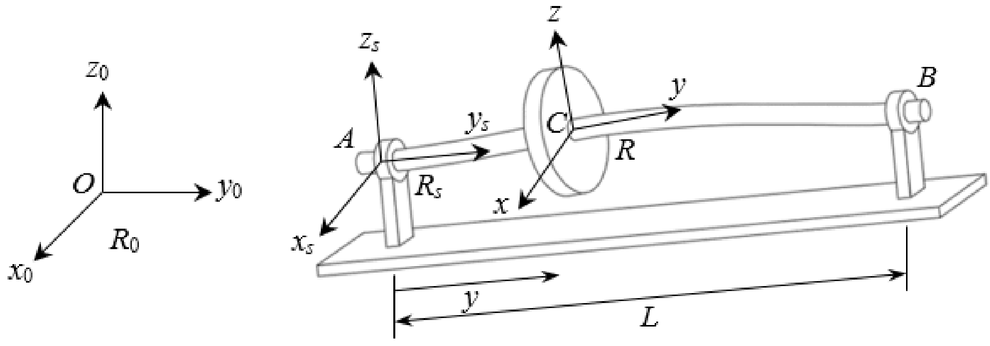

Figure 1: Schematic representation of an onboard rotor (Duchemin, 2003).

The movement of the frame R with respect to R_s is described by the angles ψ, θ, and φ. The orientation of R is defined from a rotation ψ around z_s, a subsequent rotation θ around the new direction x_1, and last by an amount φ around y, as presented by Fig. (2a). Thus, the angular velocity of the frame R with respect to R_s is given by Eq. (1).

$$\vec{\Omega}_R^{R_s} = \begin{Bmatrix} 0 \\ 0 \\ \dot{\psi} \end{Bmatrix}_{R_s} + \begin{Bmatrix} \dot{\theta} \\ 0 \\ 0 \end{Bmatrix}_{R_2} + \begin{Bmatrix} 0 \\ \dot{\phi} \\ 0 \end{Bmatrix}_{R} = \begin{Bmatrix} \dot{\theta}\cos\phi - \dot{\psi}\cos\theta\sin\phi \\ \dot{\phi} + \dot{\psi}\sin\theta \\ \dot{\theta}\sin\phi + \dot{\psi}\cos\theta\cos\phi \end{Bmatrix} \tag{1}$$

where R_2 is an intermediate frame resulting from the imposed angular rotations (Lalanne and Ferraris, 1998).

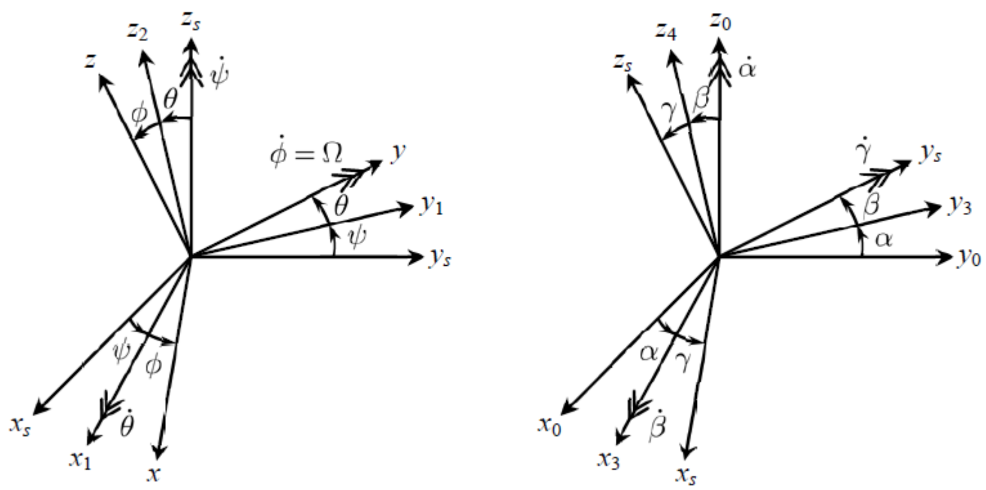

Figure 2: Reference frames for the disc and for the rotor base.

The movement of the base (i.e., frame R_s) with respect to R_0 is defined by the coordinates x_A, y_A, and z_A, and the angles α, β, and γ. The orientation of R_s is defined from a rotation α around z_0, a subsequent rotation β around the new direction x_3, and last by an amount γ around y, as presented by Fig. (2b). Thus, the vector which define the location of the point A (see Fig. (1)) and angular velocity of the frame R_s with respect to R_0 are given by Eq. (2) and Eq. (3), respectively.

$$\overrightarrow{OA} = \begin{Bmatrix} x_A \\ y_A \\ z_A \end{Bmatrix}_{R_0} = \begin{Bmatrix} x_A\cos\alpha + y_A\sin\alpha \ \cos\gamma - \ z_A\cos\beta + \ x_A\sin\alpha - y_A\cos\alpha \ \sin\beta \ \sin\gamma \\ z_A\sin\beta - \ x_A\sin\alpha - y_A\cos\alpha \ \cos\beta \\ x_A\cos\alpha + y_A\sin\alpha \ \sin\gamma + \ z_A\cos\beta + \ x_A\sin\alpha - y_A\cos\alpha \ \sin\beta \ \cos\gamma \end{Bmatrix}_{R_s} = \begin{Bmatrix} X \\ Y \\ Z \end{Bmatrix}_{R_s} \tag{2}$$

$$\vec{\Omega}_{R_s}^{R_0} = \begin{Bmatrix} 0 \\ 0 \\ \dot{\alpha} \end{Bmatrix}_R + \begin{Bmatrix} \dot{\beta} \\ 0 \\ 0 \end{Bmatrix}_{R_3} + \begin{Bmatrix} 0 \\ \dot{\gamma} \\ 0 \end{Bmatrix}_{R_s} = \begin{Bmatrix} \dot{\beta}\cos\gamma - \dot{\alpha}\cos\beta\sin\gamma \\ \dot{\gamma} + \dot{\alpha}\sin\beta \\ \dot{\beta}\sin\gamma + \dot{\alpha}\cos\beta\cos\gamma \end{Bmatrix}_{R_s} = \begin{Bmatrix} \dot{\alpha}_s \\ \dot{\beta}_s \\ \dot{\gamma}_s \end{Bmatrix}_{R_s} \tag{3}$$

The lateral vibration of the shaft (i.e., movement of frame R fixed to the disk with respect to frame R_s) is described by the translations u and w along x_s and z_s directions, respectively. Additionally, the angles θ and ψ lead to the angular orientation of the shaft with respect to the same directions x_s and z_s, respectively (Duchemin, Berlioz, Ferraris, 2006). Thus, the kinetic energy T_D of the disc (see Fig. (1)) can be derived from Eq. (4).

$$T_D = \frac{1}{2} M_D \; \vec{V}_{CR_s}^{R_0} \;^2 + \frac{1}{2} \vec{\Omega}_R^{R_0} I_D \vec{\Omega}_R^{R_0} \tag{4}$$

where M_D is the mass of the disc, $\vec{V}_{CR_s}^{R_0}$ is the translational velocity of the disc with respect to R_0 expressed in R_s, $\vec{\Omega}_R^{R_0}$ is the angular velocity vector of the frame R with respect with R_0, and I_D is the tensor of mass inertia moments.

$$\vec{V}_{CR_s}^{R_0} = \left(\frac{d\overrightarrow{OC}}{dt}\right)_{R_s} + \vec{\Omega}_{R_s}^{R_0} \times \; \overrightarrow{OC} \;_{R_s} = \begin{Bmatrix} \dot{X} + \dot{u} + \dot{\beta}_s \;\; Z + w \;\; - \dot{\gamma}_s \;\; Y + y \\ \dot{Y} + \dot{\gamma}_s \;\; X + u \;\; - \dot{\alpha}_s \;\; Z + w \\ \dot{Z} + \dot{w} + \dot{\alpha}_s \;\; Y + y \;\; - \dot{\beta}_s \;\; X + u \end{Bmatrix}_{R_s} = \begin{Bmatrix} \dot{u}_C \\ \dot{v}_C \\ \dot{w}_C \end{Bmatrix}_{R_s} \tag{5}$$

$$\vec{\Omega}_R^{R_0} = \vec{\Omega}_{R_s}^{R_0} + \vec{\Omega}_R^{R_s} = \begin{Bmatrix} \dot{\alpha}_s \\ \dot{\beta}_s \\ \dot{\gamma}_s \end{Bmatrix}_{R_s} + \begin{Bmatrix} 0 \\ 0 \\ \dot{\psi} \end{Bmatrix}_{R_s} + \begin{Bmatrix} \dot{\theta} \\ 0 \\ 0 \end{Bmatrix}_{R_2} + \begin{Bmatrix} 0 \\ \dot{\phi} \\ 0 \end{Bmatrix}_R = \begin{Bmatrix} \omega_x \\ \omega_y \\ \omega_z \end{Bmatrix}_R \tag{6}$$

$$I_D = \begin{bmatrix} I_{Dx} & 0 & 0 \\ 0 & I_{Dy} & 0 \\ 0 & 0 & I_{Dz} \end{bmatrix} \tag{7}$$

being I_{Dx}, I_{Dy}, and I_{Dz}, the mass inertia moments of the disc. ω_x, ω_y, and ω_z, are the angular velocities of the frame R with respect to the frame R_0 (Duchemin, 2003).

The kinetic energy expressions for the shaft and unbalanced mass m_u are given by:

$$T_S = \frac{1}{2}\rho S \int_0^L \; \dot{u}_s^2 + \dot{v}_s^2 + \dot{w}_s^2 \;\; dy + \frac{1}{2}\rho \int_0^L \left[I_x \, \omega_x^2 + I_y \omega_y^2 + I_z \, \omega_z^2 \right] dy$$

$$T_u = \frac{1}{2} m_u \; \vec{V}_{DR_s}^{R_0} \;^2 \tag{8}$$

where T_S and T_u are the kinetic energies of the shaft and unbalanced mass, respectively. The translations u_s, v_s, and w_s, are similar to the ones presented by Eq. (5) (i.e., time derivatives of u_C, v_C, and w_C, respectively), regarding any y position along the shaft (see Fig. (1)). I_x, I_y, and I_z, are the area inertia moments of the shaft. The parameter ρ is the volumetric density of the shaft material, E is the Young's Modulus, and S stands to the cross-section area of the shaft. Additionally,

$$\vec{V}_{DR_s}^{R_0} = \left(\frac{d\overrightarrow{OD}}{dt}\right)_{R_s} + \vec{\Omega}_{R_s}^{R_0} \times \; \overrightarrow{OD} \;_{R_s} = \begin{Bmatrix} \dot{X} + \dot{u} + d\Omega\cos\Omega t + \dot{\beta}_s \;\; Z + w + d\Omega\cos\Omega t \;\; - \dot{\gamma}_s \;\; Y + y \\ \dot{Y} + \dot{\gamma}_s \;\; X + u + d\Omega\sin\Omega t \;\; - \dot{\alpha}_s \;\; Z + w + d\Omega\cos\Omega t \\ \dot{Z} + \dot{w} - d\Omega\sin\Omega t + \dot{\alpha}_s \;\; Y + y \;\; - \dot{\beta}_s \;\; X + u - d\Omega\sin\Omega t \end{Bmatrix}_{R_s} \tag{9}$$

where $\vec{V}_{DR_s}^{R_0}$ is the translational velocity of the point D with respect to R_0 expressed in R_s (see Fig. (3)), Ω is the rotation speed of the rotor, t is the time vector, and d is the distance of m_u from the geometric center of the shaft.

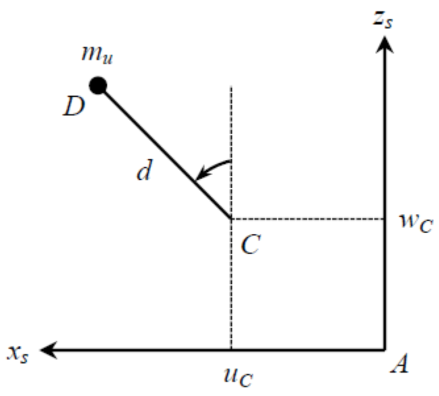

Figure 3: Unbalanced mass.

It is worth mentioning that the strain energy U of the shaft is not modified by the movement of the rotor base (i.e., translations and rotations), since it is independent from the constraints associated with the onboard rotor problem. Thus,

$$U = \frac{1}{2} EI_m \int_0^L \left[\left(\frac{\partial^2 u}{\partial y^2} \right)^2 + \left(\frac{\partial^2 w}{\partial y^2} \right)^2 \right] dy + \frac{1}{2} EI_a \int_0^L \left\{ \left[\left(\frac{\partial^2 w}{\partial y^2} \right)^2 - \left(\frac{\partial^2 u}{\partial y^2} \right)^2 \right] \cos 2\Omega t + 2 \frac{\partial^2 u}{\partial y^2} \frac{\partial^2 w}{\partial y^2} \cos 2\Omega t \right\} dy$$

$$I_m = \frac{I_x + I_z}{2} \qquad I_a = \frac{I_x - I_z}{2} \tag{10}$$

where E is the Young's Modulus associated with the shaft material.

The FE model of the shaft is elaborated based on the Timoshenko's beam theory, considering two nodes per element and four degrees of freedom per node, as presented by Fig. (4) (i.e., displacements u_1, u_2, w_1, and w_2; and angular rotations θ_1, θ_2, ψ_1, and ψ_2).

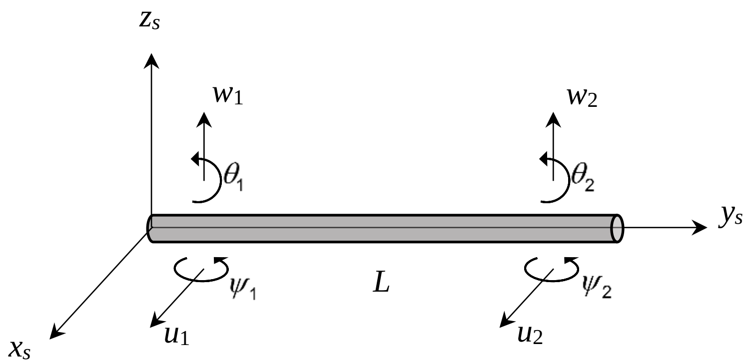

Figure 4: Degrees of freedom associated with the FE of the shaft.

The vector of nodal degrees of freedom of the shaft is given by:

$$\mathbf{q} = u_1 \quad w_1 \quad \theta_1 \quad \psi_1 \quad u_2 \quad w_2 \quad \theta_2 \quad \psi_2 \;^T \tag{11}$$

The elementary matrices associated with the FE model of the shaft are obtained by introducing the well-known shape functions (associated with the Timoshenko's beam theory) in Eq. (8) and Eq. (10) (Timoshenko, 1951). The Lagrange's equations can be applied, and the equations of motion are derived as follows:

$$\mathbf{M}\ddot{\mathbf{q}} + \left[\mathbf{D} + \mathbf{D}^* \right] \dot{\mathbf{q}} + \left[\mathbf{K} + \mathbf{K}^* \right] \mathbf{q} = \mathbf{W} + \mathbf{F}(t) + \mathbf{F}^*(t) \tag{12}$$

The matrices **M**, **K**, and **D**, are the mass, stiffness, and gyroscopic/damping of the rotor system, respectively. All these matrices are related to the shaft and the discs of the rotor, considering the base at rest. The contribution of the discs on the dynamic behavior of the rotor system is incorporated in Eq. (12) from the kinetic energy presented in Eq. (4), considering the four degrees of freedom associated with a given node of the shaft FE model (Duchemin, 2003). The additional terms associated with the motion of the base are incorporated into the matrices **D*** and **K***, as well as in the force vector **F***. The vector **F** contains the unbalance forces. **W** stands for the weight of the rotating parts.

The direct numerical integration of Eq. (12) is not possible, as it consists of a nonlinear, second-order differential system of equations. Hence, to obtain the vibration responses of the onboard rotor system, the Newton-Raphson method is considered in conjunction with the Newmark-type trapezoidal rule integration algorithm. This integration process is presented in details by Cavalini Jr et al. (2015a) in the appendix section. The detailed parameters used in the integration procedure, such as the Courant number and convergence scheme, can also be found in the aforementioned paper.

3. NUMERICAL APPLICATION

In this section, the dynamic behavior of the presented FE model is evaluated considering different base excitations. Figure (5) shows the vibration responses of the rotor system considering the fixed and excited conditions for its base. The vibration responses were determined along the x_s and z_s directions at the measurement plane S_8. In this case, two different excitations were applied (i.e., displacement of the rotor base along the x_0 and z_0 directions; Fig. (5a) and Fig. (5c), respectively). Figure (5c) presents a displacement curve which mimics the dynamic behavior of aircraft wings during a typical flight envelope. It is important to point out that the simulation time and the displacement amplitude does not match with real excitations applied to aircrafts during flights. In this context, the vibration responses associated with each excitation curves are shown by Fig. (5b) and Fig. (5d) (excitations Fig. (5a) and Fig. (5c), respectively; full simulation time of 10 s in steps of 0.001 s). The maximum base accelerations along the x_s and z_s directions were 1.5 m/s^2 and 10 m/s^2, respectively. The operational rotation speed of the rotor Ω was fixed at 1200 rev/min and an unbalance level of 487.5 g.mm / 0° was applied to the disc D_1. Note that the vibration responses of the rotor system changed according to the imposed base displacements. As expected, the vibration responses determined along the x_s direction is bigger than the one obtained along the z_s direction when the displacement of the base applied along the x_0 direction is considered (and vice-versa). Similar results were found considering the vibration responses measured at the plane S_{28}.

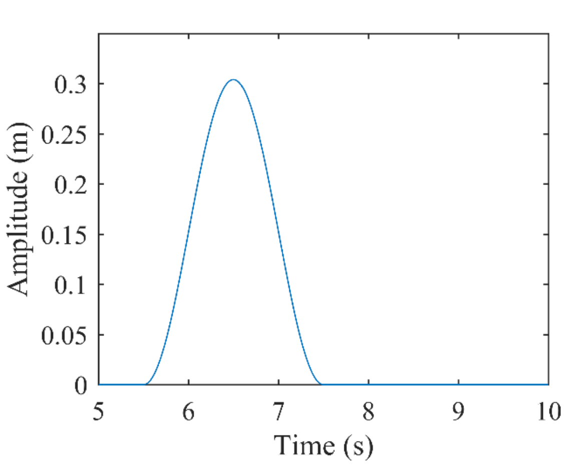

a) Excitation along the x_0 direction.

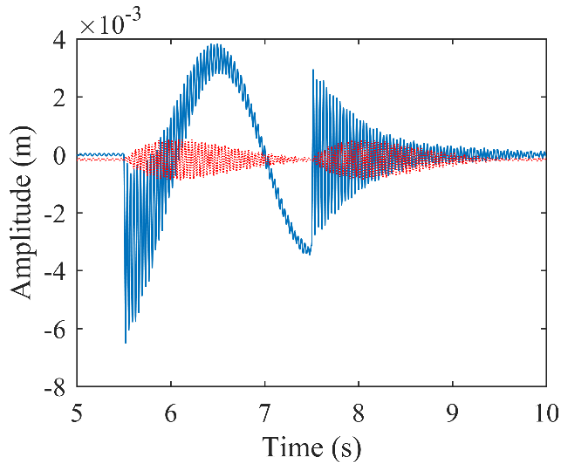

b) x_s direction (----) and z_s direction (----).

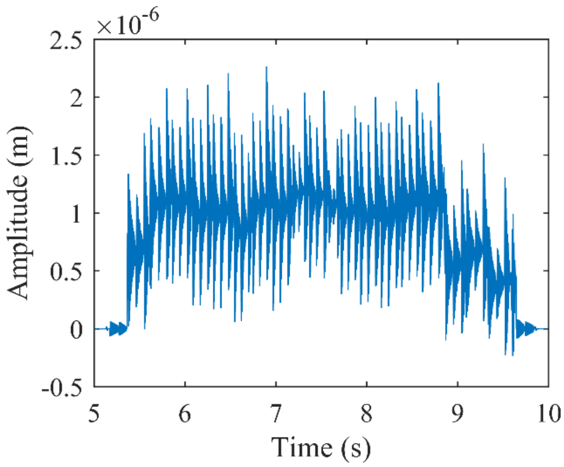

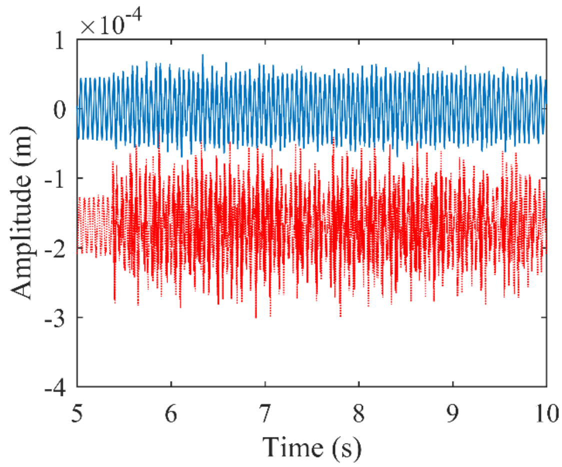

c) Excitation along the z_0 direction. d) x_s direction (----) and z_s direction (----).

Figure 5: Vibration responses determined at the plane S_8 of the rotor considering different base excitations.

Figure (6) shows the orbits of the rotor system determined at the measurement plane, considering a sinusoidal excitation imposed around the direction x_s as given by:

$$\ddot{\alpha}_s = \Lambda \sin\left(n \frac{2\pi\Omega}{60} t \right) \tag{13}$$

where Λ was fixed as being equal to 0.5 rad/s^2 and n is a constant used to produce the super synchronous base excitations. In this case, n = 2, 3, 4, and 5 (Fig. (6a), (6b), (6c), and (6d), respectively). The scales used for the x_s and z_s directions are different to provide a better visualization of the dynamic effects on the rotor orbits. A high excitation amplitude was used to better visualize its effect in the orbits of the rotor. The operational rotation speed of the rotor Ω was kept at 1200 rev/min and an unbalance level of 487.5 g.mm / 0° was applied to the disc D_1. Note that the shape of the rotor orbits changes according to the imposed base movement. Similar results were found considering the vibration responses measured at the plane S_{28}.

4. CONCLUSION

In this paper, an investigation regarding the dynamic behavior of a rotor system subjected to base excitation was discussed. The rotating machine used in the numerical analysis is composed by a horizontal flexible shaft, two rigid discs, and two self-aligning ball bearings. The mathematical model of the rotor was presented through Eq. (1) to (12), enabling the development of the FE method. The proposed analysis was performed both in the time and frequency domains, as represented by the orbits, unbalance responses, and the FRFs of the rotor system. The vibration responses were determined from different base excitations, so that the discrepancies between regular rotor and onboard rotor were analyzed. The transient dynamic behavior of the system was not taken into account in this contribution. Therefore, further studies will encompass the vibration responses of the onboard rotor system operating in run-up and run-down conditions. An experimental verification is also scheduled.

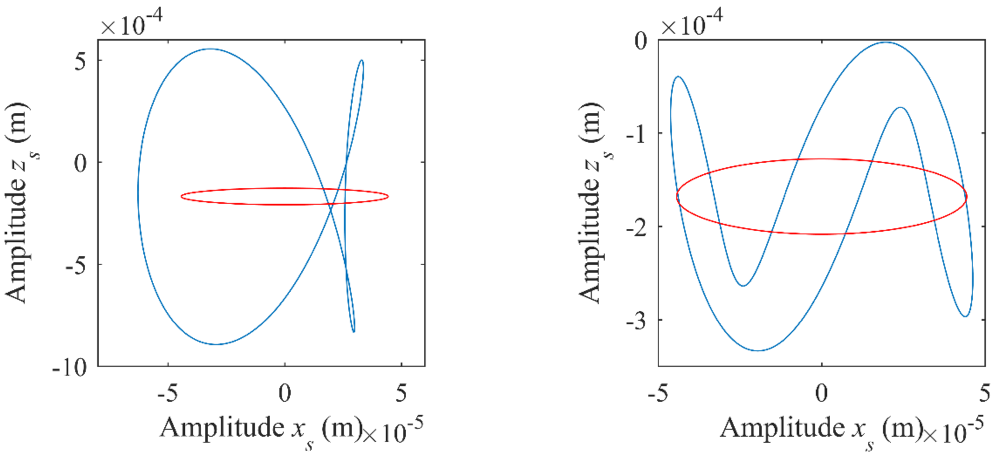

a) n = 2. b) n = 3.

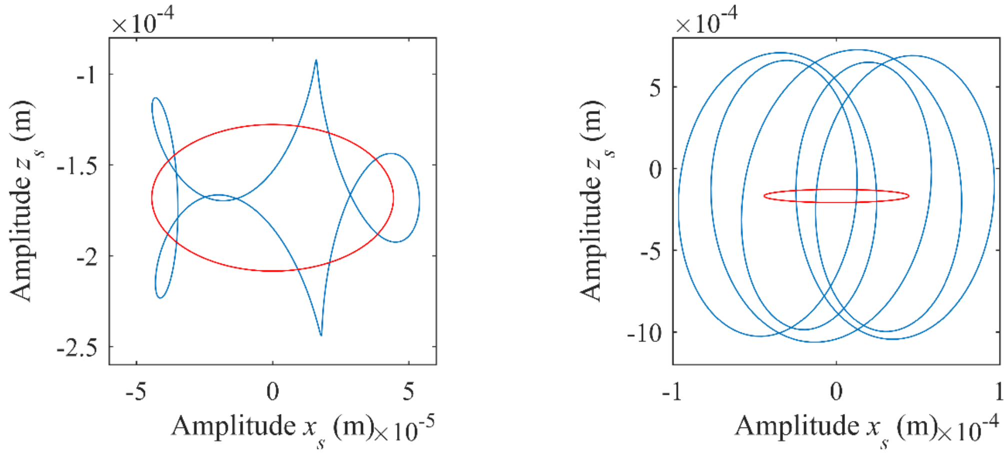

c) n = 4. d) n = 5.

Figure 6: Orbits determined at the measuring plane S_8 considering sinusoidal super synchronous base excitations according to the rotation speed of the rotor (---- base at rest; ---- base excitation)

5. ACKNOWLEDGEMENTS

The authors are thankful to the Brazilian Research Agencies CAPES, CNPq (574001/2008-5) and FAPEMIG (TEC-APQ-022284-15 / TEC-APQ-307609) for the financial support provided to this research effort.

6. REFERENCES

Cavalca, K.L., Cavalvante, P.F., Okabe, E.P., 2005, “An investigation on the influence of the supporting structure on the dynamics of the rotor system”. Mechanical Systems and Signal Processing, Vol. 19, n. 1, p. 157-174.

Cavalini Jr., A.A., Lara-Molina, F.A., Sales. T.P., Koroishi, E.H., Steffen Jr, V., 2015a, “Uncertainty analysis of a flexible rotor supported by fluid film bearings”. Latin American Journal of Solids and Structures, Vol. 12, No. 8, pp. 1487-1504.

Cavalini Jr., A.A., Lobato, F.S., Koroishi, E.H., Steffen Jr, V., 2015b, “Model updating of a rotating machine using the self-adaptive differential evolution algorithm”. Inverse Problems in Science and Engineering, Vol. 24, No. 3, pp. 504-523.

Dakel, M., Baguet, S., Dufour, R., 2014, “Steady-state dynamic behavior of an on-board rotor under combined base motions”. Journal of Vibration and Control, Vol. 20, n. 15, p. 2254-2287.

Das, A.S., Dutt, J.K., Ray, K., 2010, “Active vibration control of unbalanced flexible rotor-shaft systems parametrically excited due to base motion”. Applied Mathematical Modelling, Vol. 34, n. 1, p. 2353-2369.

Duchemin, M., 2003, “Contribuition à l’étude du comportement dynamic d’un rotor embarqué”. PhD thesis, INSA Lyon, Lyon.

Duchemin, M., Berlioz, A., Ferraris, G., 2006, “Dynamic behavior and stability of a rotor under base excitation”. ASME Journal of Vibration and Acoustics, Vol. 128, p. 576.

El-Saeidy, F.M.A., Sticher, F., 2010, “Dynamics of a rigid rotor linear/nonlinear bearings system subject to rotating unbalance and base excitations”. Journal of Vibration and Control, Vol. 16, n. 3, p. 403-438.

Hori, Y., Kato, T., 1990, “Earthquake-induced instability of a rotor supported by oil film bearings”. ASME Journal of Vibration and Acoustics, Vol. 112, n. 2, p. 160-165.

Lalanne, M., Ferraris, G., 1998, “Rotordynamics prediction in engineering”. John Wiley & Sons, INC.

Lei, H., Yushu, C., 2014, “Dynamical simulation and load control of a Jeffcott rotor system in Herbst maneuvering flight”. Journal of Vibration and Control, Vol. 1, n. 1, p. 1-14.

Marx, S., Nataraj, C., 2007, “Suppression of base excitaion of rotors on magnetic bearings”. International Journal of Rotating Machinery, Vol. 1, n. 1, p. 1-10.

Storn, R., Price, K., 1995, “Differential evolution: a simple and efficient adaptive scheme for global optimization over continous spaces”. International Computer Science Institute, Vol. 12, No. 1, pp. 1-16.

Timoshenko, S.; Goodier, J. N. Theory of Elasticity. 2nd Edition. ed. New York: McGraw Hill, 1951.

7. RESPONSIBILITY NOTICE

The authors are the only responsible for the printed material included in this paper.